Comparison of dissipative particle dynamics and Langevin thermostats for out-of-equilibrium simulations of polymeric systems

C. Pastorino,[1,2] T. Kreer,[3] M. Müller,[4] and K. Binder[2]

[1]*Departamento de Física, Centro Atómico Constituyentes, CNEA/CONICET, Av. Gral. Paz 1499,*
1650 Provincia de Buenos Aires, Argentina
[2]*Institut für Physik WA331, Johannes Gutenberg-Universität, 55099, Mainz, Germany*
[3]*Institut Charles Sadron, 6 Rue Boussingault, 67083 Strasbourg, France*
[4]*Institut für Theoretische Physik, Friedrich-Hund-Platz 1, 37077 Göttingen, Germany*

In this work we compare and characterize the behavior of Langevin and dissipative particle dynamics (DPD) thermostats in a broad range of nonequilibrium simulations of polymeric systems. Polymer brushes in relative sliding motion, polymeric liquids in Poiseuille and Couette flows, and brush-melt interfaces are used as model systems to analyze the efficiency and limitations of different Langevin and DPD thermostat implementations. Widely used coarse-grained bead-spring models under good and poor solvent conditions are employed to assess the effects of the thermostats. We considered equilibrium, transient, and steady state examples for testing the ability of the thermostats to maintain constant temperature and to reproduce the underlying physical phenomena in nonequilibrium situations. The common practice of switching off the Langevin thermostat in the flow direction is also critically revisited. The efficiency of different weight functions for the DPD thermostat is quantitatively analyzed as a function of the solvent quality and the nonequilibrium situation.

PACS number(s): 02.70.Ns, 05.70.Ln, 71.20.Rv, 05.10.−a

I. INTRODUCTION

The need and use of thermostats in computer simulations started with the beginning of the field itself. The original molecular dynamics (MD) method, intended for microcanonical ensemble simulations, was soon extended to different ensembles in order to mimic conditions in which experiments are actually performed. The thermostat in MD simulations implies the assumption that the system transports heat "instantaneously" fast on the spatial scale of the simulation. Even when this is arguably not completely correct in a real system, many studies are faced with the situation of performing simulations at constant temperature as a way of obtaining a physically meaningful condition.

It is a nontrivial challenge to achieve a constant temperature in a simulation of driven soft matter systems, such as polymer brushes interacting with flowing polymer melts, which we consider in the present work.

In this work, we present simulation data which we obtained by integrating Langevin-like equations with the standard MD integrators using either a Langevin (LGV) or a dissipative particle dynamics (DPD) thermostat to maintain temperature. This is often called *stochastic dynamics* (SD) or *Brownian dynamics* (BD) [1–3], but we address a physical regime in which the friction and stochastic forces, added to the conservative forces of the system, are small enough in order not to significantly perturb the natural dynamics of the polymeric system. This is typically achieved by using the smallest possible value for the friction constant, γ, providing that the temperature is conserved under the desired physical conditions. This approach also requires that the system has intermediate to high monomer densities to warrant that the friction due to the conservative interactions is significantly larger than the frictional and random forces arising from the thermostat. The regime of dilute polymer solutions is ex-cluded from this study because, in this case, the polymer-solvent interactions are important for the local dynamics of the molecules.

In this sense we consider the Langevin and DPD frictional and stochastic forces as *thermostats* that are added to the true conservative forces of the system, as it is generally employed in MD. This physical regime is of great interest for a number of soft matter systems, such as polymeric interfaces, blends, and melts, which are successfully studied in the framework of coarse-grained models [4–7].

This is the case, for example, in soft matter systems in which usually the thermostat keeps the temperature constant and additionally takes account of the action of solvent particles that are not explicitly modeled in the simulation.

A case which has attracted abiding interest is the simulation of out-of-equilibrium phenomena in which a rate of energy must be injected into the system to drive it out of equilibrium. This energy must be removed in order to keep the temperature constant, and this is usually done by the action of a thermostat. There are excellent reviews that describe the different types of thermostats and their respective advantages and limitations for studying various systems and physical phenomena [1,3,8]. Of course, it is crucial that the dynamical behavior observed in a simulation faithfully represents the actual dynamics of the desired system and is essentially free from artifacts introduced by the thermostat. This issue shall be explored for out-of-equilibrium simulations of polymeric systems in our study.

In this paper, we focus on the behavior of Langevin and DPD [9–12] thermostats for a range of typical polymeric systems in nonequilibrium conditions. The former has been widely used in equilibrium simulations but is known to have undesirable properties, such as screening of hydrodynamic interactions and lack of Galilean invariance [7,13], in nonequilibrium situations. A typical work-around when using the

Langevin thermostat for nonequilibrium simulations consists in switching off the thermostat in the direction in which non-conservative external forces are applied to the system or applying it only in one spatial direction. In this way one recovers momentum conservation in the shear direction, while conserving the temperature by applying the thermostat in the perpendicular direction in which no direct nonconservative force is applied [5,6,14].

The DPD scheme only recently has started to be utilized as a stand-alone thermostat [7,15]. It was originally developed as a method for performing mesoscale simulations by combining this thermostat and very "soft" potentials. The latter allow for the use of a large time step in MD simulations [9–11]. The maximal time step that is permissible in DPD simulations has been investigated thoroughly [8,16–18]. Utilizing a DPD thermostat in conjunction with "hard" potentials—typical of coarse-grained models widely used for polymers and other condensed matter systems [19]—one loses this advantage, and one must take a time step on the order of that typically used in MD simulations of coarse-grained models. The local conservation of momentum and the Galilean invariance, however, are inherited from the original DPD method, and possibly this is a great advantage.

In the following, we consider three polymeric systems to assess the effects of two versions of Langevin thermostats (with and without switching off the thermostat in the flow direction) and the DPD thermostat: (a) single end-grafted polymer layers (so-called polymer brushes), (b) two opposing and interdigitating polymer brushes, and (c) a brush-melt interface, which exhibits a rich wetting behavior. The equilibrium properties of these reference systems are interesting and have been comprehensively studied in previous works [4,15,20–24]. The brush layers are characterized by the number of grafted chains per unit area or grafting density ρ_g. Typical equilibrium density profiles for these three systems are shown in Fig. 1. Additionally, a simple bulk system of a polymeric liquid with periodic boundary conditions in all three directions was considered.

These systems are also of great interest out of equilibrium, for instance, because of the surprisingly small friction of two opposing brushes sliding past each other [21,25,26].

The interface between a brush and a melt of identical chains is a prototypical example for a copolymer-laden interface or a melt in contact with a soft, elastically deformable substrate (e.g., confining brush-coated walls of a channel) [15]. In addition to the rich wetting properties, typical applications (e.g., droplet breakup in a polymer blend under shear or flow in a microfluidic channel) involve flow and shear at the brush-melt interface. Therefore, the study of boundary conditions and the rheological properties of the macromolecular liquid subjected to different types of flows make the nonequilibrium properties of this system particularly interesting.

The behavior of the thermostats in equilibrium, transient, and different kinds of steady states was tested in a wide number of typical situations that can be encountered in simulations. Also, Poiseuille and Couette flows of the polymeric liquid were considered to compare different weight functions of the DPD thermostat.

The details of the thermostats and the polymer model are explained in Sec. II. Section III presents the discussion of
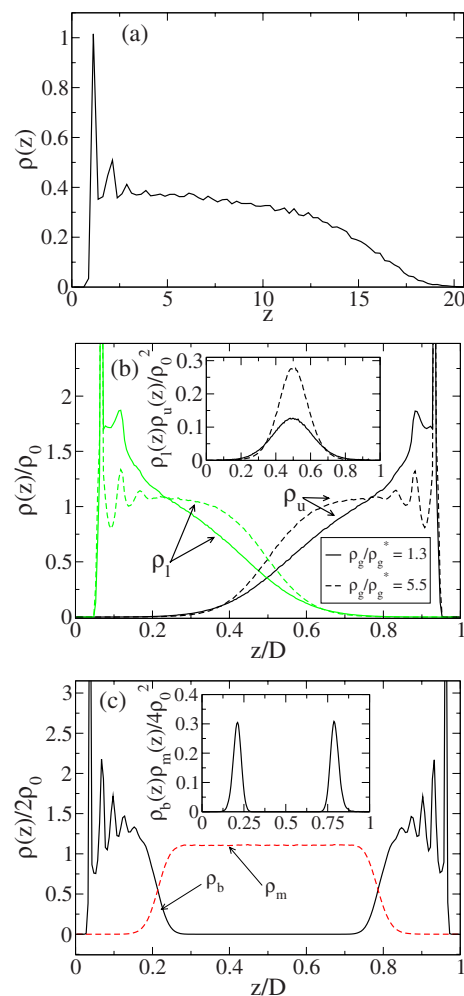

FIG. 1. (Color online) Equilibrium density profiles for the three systems under consideration: (a) single brush layer, (b) two opposing brush layers in interaction at two different grafting densities, and (c) brush-melt interfaces. The insets show the product of upper and lower brush density profiles $\rho_u \times \rho_l$ (b) or the product of brush and melt phases $\rho_b \times \rho_m$ (c), accounting for the level of interdigitation of the different phases. In all cases, the temperature is $T = 1.68$. The chain length is $N = 30$ for cases (a) and (b) and $N = 10$ for case (c). The distance between the grafted beads of the opposing brushes is $D = 17.5$ for case (b) and $D = 30$ for case (c). The normalization is given by $\rho_0 = \rho_g / D$.

our results, which begins with a quantitative study of the relative strengths of thermostats for a given set of parameters. Section III is divided into sections corresponding to each different system. The analysis of single-brush layer transient states is presented in Sec. III A, and the steady state of two polymer brushes in relative sliding motion is discussed in Sec. III B for two different grafting densities. In this way, we address two regimes: concentrated solution or melt in which hydrodynamic interactions are screened and a more dilute regime. Finally, the study of different DPD weight functions and their efficiency for conserving the temperature in the strong out-of-equilibrium regime for Couette and Poiseuille flows of the brush-melt interface is described in Sec. III C. Discussion and concluding remarks are presented in Sec. IV.

II. POLYMER MODEL AND THERMOSTAT DETAILS

A. Coarse-grained model

We used a well-established coarse-grained bead-spring model [19] for polymers with excluded volume and intramolecular interactions. This model has been applied to a variety of thermodynamic conditions, chain lengths, and physical regimes, such as glasses, melts, dilute solutions, etc. [4,27–29]. The interaction between neighboring beads along the same polymer is modeled by a finite extensible nonlinear elastic (FENE) potential,

$$U_{\text{FENE}} = \begin{cases} -\dfrac{1}{2} k\, R_0^2 \ln\left[1 - \left(\dfrac{r}{R_0} \right)^2 \right], & r \le R_0 \\ \infty, & r > R_0 \end{cases}, \qquad (1)$$

where the maximum allowed bond length is $R_0 = 1.5\sigma$, the spring constant is $k = 30\varepsilon/\sigma^2$, and $r = |\mathbf{r}_i - \mathbf{r}_j|$ denotes the distance between neighboring monomers. Excluded volume interactions at short distances and van der Waals attractions between segments are described by a truncated and shifted Lennard-Jones (LJ) potential,

$$U(r) = U_{\text{LJ}}(r) - U_{\text{LJ}}(r_c) \qquad (2)$$

with

$$U_{\text{LJ}}(r) = 4\varepsilon\left[\left(\frac{\sigma}{r} \right)^{12} - \left(\frac{\sigma}{r} \right)^6 \right], \qquad (3)$$

where the LJ parameters, $\varepsilon = 1$ and $\sigma = 1$, define the units of energy and length, respectively. The temperature is therefore given in units of ε/k_B, with k_B the Boltzmann constant. $U_{\text{LJ}}(r_c)$ is the LJ potential evaluated at the cutoff radius. We considered two values as cutoff distance: (i) 2 times the minimum of the LJ potential, $r_c = 2 \times 2^{1/6} \simeq 2.24\sigma$, which allows us to consider poor solvent conditions; (ii) $r_c = 2^{1/6} \simeq 1.12\sigma$, which models good solvent conditions. In the latter case, the interactions between monomers of different chains are purely repulsive [21–23], whereas in the former case, longer ranged attractions are included giving rise to liquid-vapor phase separation and droplet formation [30,31] below the Θ temperature, $\Theta = 3.3\varepsilon/k_B$. We analyze the efficiency of the thermostats for both cases.

The substrate is modeled as an idealized flat and impenetrable wall, which interacts with the polymer segments via an integrated Lennard-Jones potential,

$$V_{\text{wall}}(z) = |A|\left(\frac{\sigma}{z} \right)^9 - A\left(\frac{\sigma}{z} \right)^3, \qquad (4)$$

where $A = 3.2\varepsilon$, used throughout this work, is sufficient to make the liquid wet the bare substrate [31,32]. The tethered beads are fixed randomly in the grafting plane at a distance of 1.2σ from the wall position for all the cases. In the following, we will use LJ units [1] for all quantities, unless explicitly mentioned otherwise.

B. Langevin and dissipative particle dynamics thermostats

Both, Langevin and DPD thermostats can be written in a general form, starting from the Hamiltonian equations of motion [1,8],

$$\dot{\mathbf{r}}_i = \frac{\mathbf{p}_i}{m_i},$$

$$\dot{\mathbf{p}}_i = \mathbf{F}_i + \mathbf{F}_i^D + \mathbf{F}_i^R, \qquad (5)$$

where $\mathbf{F}_i$ is the total conservative force on each particle and m_i is the mass of each particle. $\mathbf{F}_i^D$ and $\mathbf{F}_i^R$ are the forces due to the thermostat and will be of different forms for the Langevin and the DPD cases. The difference between DPD and Langevin thermostats is the way in which random and dissipative forces are applied.

In the case of Langevin thermostats, the dissipative force on particle i is given by $\mathbf{F}_i^D = -\gamma \mathbf{v}_i$, where γ is the friction coefficient and $\mathbf{v}_i$ is the particle velocity. The random force, $\mathbf{F}_i^R$, has zero mean value and its variance satisfies [3]

$$\langle F_{i\mu}^R(t) F_{j\nu}^R(t') \rangle = 2\gamma T k_B \delta_{ij} \delta_{\mu\nu} \delta(t - t'), \qquad (6)$$

where the indices i and j label particles, μ and ν are Cartesian components, and T is the temperature at which the system is simulated.

For the DPD case [9,10], the dissipative and frictional forces are applied in a pairwise form, such that the sum of thermostatting forces acting on a particle pair equals zero. The expression for the forces is the following:

$$\mathbf{F}_i^D = \sum_{j(\neq i)} \mathbf{F}_{ij}^D, \quad \mathbf{F}_{ij}^D = -\gamma \omega^D(r_{ij})(\hat{\mathbf{r}}_{ij} \cdot \mathbf{v}_{ij})\hat{\mathbf{r}}_{ij},$$

$$\mathbf{F}_i^R = \sum_{j(\neq i)} \mathbf{F}_{ij}^R, \quad \mathbf{F}_{ij}^R = \sigma \omega^R(r_{ij}) \theta_{ij} \hat{\mathbf{r}}_{ij}, \qquad (7)$$

where for each vector $\mathbf{a}$ we define $\mathbf{a}_{ij} \equiv \mathbf{a}_i - \mathbf{a}_j$, γ is the friction constant, and σ is the noise strength. Friction and noise, γ and σ, obey the relation $\sigma^2 = 2k_B T\gamma$, and the associated weight functions satisfy the fluctuation-dissipation theorem if the following relation is fulfilled [11]:

$$[\omega^R]^2 = \omega^D. \qquad (8)$$

θ_{ij} is a random variable with zero mean and second moment

$$\langle \theta_{ij}(t) \theta_{kl}(t') \rangle = (\delta_{ij}\delta_{jl} + \delta_{il}\delta_{jk})\delta(t - t'). \qquad (9)$$

The standard weight functions found in the literature are

$$[\omega^R]^2 = \omega^D = \begin{cases} (1 - r/r_c)^2 & r < r_c, \\ 0, & r \ge r_c \end{cases}, \qquad (10)$$

where r_c is the cutoff radius for a given molecular model. However, we emphasize that Eq. (10) is just the typical choice when the DPD thermostat is employed in conjunction with "soft" potentials. For arbitrary models, one can choose a different set of functions providing that they fulfill Eq. (8), and one can exploit this freedom to optimize the efficiency of the thermostat for "hard" potentials. In this work, we will use the standard weights, but also test other possibilities, whose forms are given in the first row of Table I. The equations of motion [Eq. (5)] were integrated using the velocity Verlet algorithm [1,8] with a time step of $dt = 0.002\tau$, where $\tau = \sigma(m/\varepsilon)^{1/2}$ denotes the time unit in terms of LJ parameters.

TABLE I. Number of thermostated particles, N_{TP}, for different weight functions using the DPD thermostat. See text and Eq. (11).

$N_{TP}(\omega^R)$	$\omega^R = 1 - \frac{r}{r_c}$	$\omega^R = \sqrt{1 - \frac{r}{r_c}}$	$\omega^R = \Theta(r_c - r)$
Good solvent ($r_c = 1.12$)	0.301	0.904	2.997
Poor solvent ($r_c = 2.24$)	6.753	12.814	28.868

III. RESULTS

In this section, the results corresponding to the three polymeric systems, whose equilibrium density profiles are shown in Fig. 1, will be analyzed. The difference between weight functions and the way random and friction forces are applied in Langevin and DPD thermostats does not allow for a direct comparison of the friction strength γ between both schemes. To obtain a direct measurement of thermostat strengths, we computed the mean friction and dissipative forces as a function of γ for a polymeric liquid of 10-bead chains in a bulk solution (using periodic boundary conditions in all spatial directions). In the case of the DPD thermostat, the standard weight functions were used [see Eq. (10)]. Figure 2 shows the total force as a function of γ. Poor and good solvent conditions exhibit quite different behaviors. In the first case, the Langevin and DPD thermostat show a very similar behavior for the whole range of γ. For good solvent conditions (only the repulsive part of the LJ potential is kept), however, the mean Langevin forces are two orders of magnitude larger than those of the corresponding DPD counterpart (for the standard choice of weight functions). This means, for example, that a friction constant $\gamma_{DPD} = 2$ is equivalent to a value of $\gamma_{LGV} = 0.01$, as regards the mean value of the "thermostat force" acting on each bead. The ratio $\frac{\langle F_{LGV} \rangle}{\langle F_{DPD} \rangle}$ as a function of γ is shown with open symbols for the sake of comparison. The reason for the big difference, in the case of good
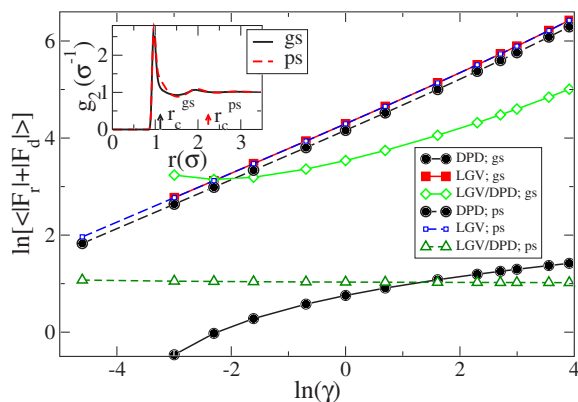

FIG. 2. (Color online) Comparison of mean random and dissipative forces for DPD and Langevin (LGV) thermostats as a function of the friction constant, γ, for a bulk system with temperature $T = 1.68$ and density $\rho = 0.61$. The ratio $\frac{\langle F_{LGV} \rangle}{\langle F_{DPD} \rangle}$ is shown in open circles for both, good solvent (gs) and poor solvent (ps) conditions. Inset: Pair correlation function $g_2(r)$ of the polymeric liquid for good (solid line) and poor (dashed line) solvent conditions. The arrows indicate the position of the cutoff radius in each case.

solvent, is the structure of the liquid and, more important, the small cutoff radius—there are very few beads in the range of the weight functions, and the standard weight functions are small in the vicinity of r_c, where most of the neighbors are located. The pair correlation functions and corresponding cutoff radii are shown in the inset of Fig. 2.

At this point, it is important to recall that the original reason for choosing those weight functions [Eq. (10)] was based on the idea of using DPD together with "soft" potentials [9,12] to achieve the largest possible time step. To this end, the thermostat forces need also to be smoothly varying functions of the position in order to have the same properties as the conservative forces. Actually, the only constraint the weight functions must fulfill is the fluctuation-dissipation theorem [9,11], i.e., Eq. (8).

We will see below that the standard choice can be even bad for nonequilibrium simulations, in which a significant amount of heat per unit time must be removed. To quantify the efficiency of the thermostat to maintain constant temperature, we define the number of thermostated particles, N_{TP}, for a given DPD weight function pair as

$$N_{TP} = \rho_0 \int_0^{r_c} \omega^R(r) g_2(r) 4\pi r^2 dr, \qquad (11)$$

where r_c is the cutoff radius of the conservative potentials which coincides with the cutoff of the weight functions for the dissipative and frictional forces. $g_2(r)$ is the pair correlation function for particles in the polymeric liquid. For the standard weight functions and good solvent conditions, N_{TP} is rather small (cf. Fig. 2).

The pair correlation functions for poor and good solvent conditions were taken from bulk simulations of a 10-bead polymeric liquid at $T = 1.68$ and $\rho = 0.61$ which corresponds to the density of a melt that coexists with its vapor [31]. In Table I the calculated values of N_{TP}, as given by Eq. (11), are shown for three different choices of weight functions. The second column shows N_{TP} for the standard weight functions [Eq. (10)]. The third column shows the square root of the usual weight functions which slightly increases the force in the region $r \lesssim r_c$. The last column corresponds to constant weight functions, i.e., $\omega^R = \omega^D = \Theta(r_c - r)$, with Θ being Heaviside's step function. The differences among the weight functions are evident from the values of N_{TP}. Different weight functions give rise to significant changes in the efficiency of the thermostat. In particular, the standard weight functions inherited from DPD models with "soft" potentials present the lowest value for N_{TP} which is significantly smaller than the values for other choices. As will be shown in Sec. III C, this is indeed an important issue in out-of-equilibrium simulations.

A. Single brush

We consider a single polymer brush layer with $N = 30$ beads per chain in equilibrium under good solvent conditions. The brush stretches freely according to the balance of entropy and steric repulsion between the monomers [4]. At time $t = 0$ a constant wall velocity of $v_x = 1$ is switched on in one direction, and the transient behavior of the brush is
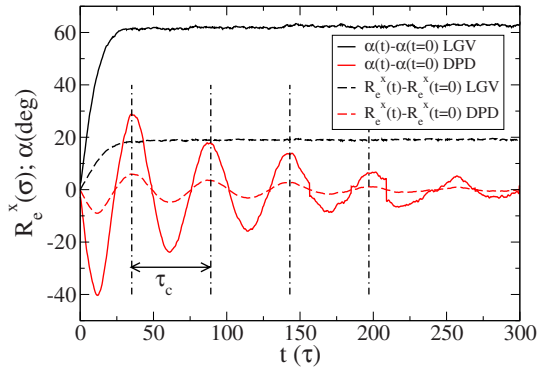
FIG. 3. (Color online) Transient evolution of the inclination angle α of the polymer brush (solid line) and the $\hat{x}$ component of the end-to-end vector R_e^x (dashed line) for Langevin and DPD thermostats. τ_c is the characteristic response time (see text and Fig. 5).

monitored. We took mean values over 10 simulations starting from independent equilibrium configurations. For each simulation, 3×10^5 to 6×10^5 steps with a time step $dt = 0.002$ were performed.

The rheological response of the polymer brush is analyzed for three different cases: the usual Langevin thermostat with the same value of γ in all spatial directions, the Langevin thermostat with zero friction constant in shear direction (denoted as $\gamma_x = 0$), and the DPD thermostat. It is known that the usual Langevin thermostat ($\gamma_x \neq 0$) does not reproduce the hydrodynamic behavior correctly because it does not conserve momentum [7,13] and biases the flow profile in shear direction. A common work-around to partially overcome these problems in nonequilibrium simulations of simple (laminar) flows is to switch off the Langevin thermostat in the direction in which external nonconservative forces are applied [7,33]. This corresponds to our second approach with $\gamma_x = 0$. Alternatively, Langevin thermostat is frequently switched off in two Cartesian components, being active only in the vorticity direction [4,5,14].

The thermostat's action can be rather understood as an implicit (fictitious) solvent acting on the polymer beads. In our coarse-grained simulation approach an effect of the implicit solvent on the dynamical properties is undesirable. As we will show in the following, however, there are cases where such effects cannot be avoided. In the case of the Langevin thermostat, this solvent is at rest in the laboratory frame. When the brush layer starts moving through the implicit solvent, the behavior of Langevin and DPD thermostats differs drastically. A first evidence of these differences is shown in Fig. 3, where Langevin and DPD thermostats are compared using a friction constant of $\gamma = 2$ in all spatial directions. The angle α between the vector normal to the substrate and the average end-to-end vector, $\mathbf{R}_e = \mathbf{r}_l - \mathbf{r}_N$, with $\mathbf{r}_l$ and $\mathbf{r}_N$ denoting the position vectors of the grafted and free end of a polymer chain, respectively, are shown as a function of time. While for the DPD thermostat α exhibits a decaying oscillatory behavior which ends in a steady state with the brush perpendicular to the wall ($\alpha = 0$), the Langevin thermostat shows an angle which monotonously increases to a steady state value of 60°. This can be understood in terms of the lack of Galilean invariance of the Langevin thermostat.
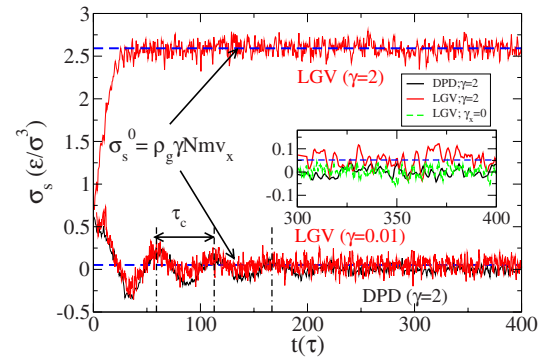

FIG. 4. (Color online) Comparison of shear stress for DPD and Langevin thermostats. For the second case two different values of γ were considered. The inset shows the systematic difference for DPD and Langevin thermostats with $\gamma = 0.01$, close to steady state, and the approach to $\sigma_s = 0$ for the Langevin thermostat with $\gamma_x = 0$ (dashed line). τ_c is similar to Fig. 3. The mean stress for Langevin is indicated with a horizontal dashed line to improve clarity.

The brush is dragged through a fictitious solvent, which is always at rest in the laboratory frame. In the case of the DPD thermostat, the Galilean invariance, which follows from momentum conservation, implies that the polymer brush at rest and in steady state is equivalent. This case provides an example where the particular thermostat implementation plays a crucial role for the dynamics of the system and can even alter the results qualitatively.

The oscillation frequency of α is a general property of the brush layer from which we can extract a characteristic response time. The component of the end-to-end vector in shear direction, R_e^x (dashed lines in Fig. 3), and the mean shear stress (force per surface area) on the grafted heads of the polymer brush (see Fig. 4) present a similar behavior. Defining for each observable $A \equiv A_0 \exp(-t/\tau_c)$, the decaying envelope of the oscillating curves, maxima and minima can be brought onto the same curve (see Fig. 5), yielding a characteristic time, $\tau_c = 53.94\tau$. The $\gamma_x = 0$ case for the Langevin thermostat (not shown) presents the same behavior as the DPD thermostat with the same characteristic time within the error.
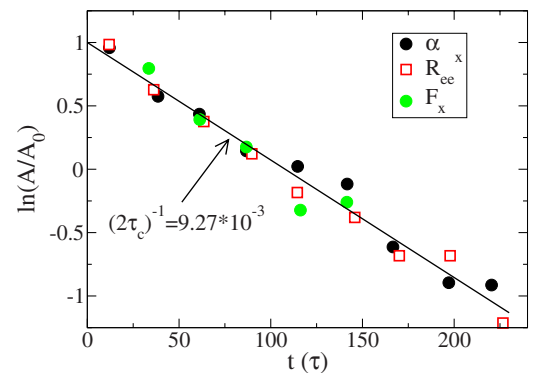

FIG. 5. (Color online) Maxima and minima of the oscillating curves (Figs. 3 and 4) for the single brush system. A characteristic frequency of the system is found when using DPD or Langevin thermostats with $\gamma = 0.01$.
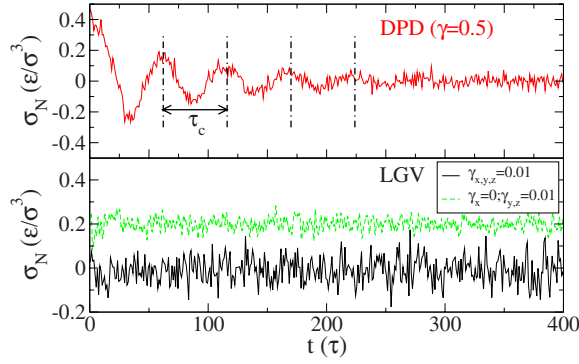
FIG. 6. (Color online) Upper panel: Normal stress as a function of time for DPD. Lower panel: Langevin thermostat with $\gamma=0.01$ in all directions and $\gamma_x=0$ along the shear direction. The curve corresponding to the latter case was shifted by 0.2 to improve clarity.

As observed for the mean thermostat forces (see Fig. 2) in the good solvent case, similar forces for Langevin and DPD thermostats are obtained for values of γ which differ by two orders of magnitude. We therefore performed the simulations for the Langevin thermostat with $\gamma=0.01$ in all spatial directions, which corresponds to $\gamma=2$ for the DPD case. Indeed, we observe the oscillations also for the Langevin thermostat for a sufficiently small value of γ (see Fig. 4). This shows that the over-damping in the previous case ($\gamma=2$) is due to the large, but not uncommon value of γ.

While the oscillations are reproduced for the smaller value of γ, the steady state shear stress remains finite. It can easily be calculated for both values of γ via

$$\sigma_s^0 = \rho_g \gamma N m v_x, \qquad (12)$$

with $m \equiv 1$ the monomer mass. As expected, the steady state for $\gamma_x=0$ yields $\sigma_s=\sigma_s^0=0$, shown as a dashed line in the inset of Fig. 4.

Figure 6 shows the transient behavior of the normal pressure exerted by the brush layer. Again, oscillations of the stress are observed for the DPD thermostat, while they are not directly observed in either version of the Langevin thermostat even for the smaller value of the friction coefficient. A Fourier frequency analysis of the time sequence, however, exhibits a peak at the same frequency for all cases.

At first one could argue that the Langevin thermostat over-damps the oscillations because local momentum is only conserved in the shear direction, and a nonequilibrium situation in which there is a strong coupling between directions cannot be faithfully reproduced. This coupling would be reinforced by the chain connectivity of the polymeric system. We found, however, that for good solvent conditions and $\gamma=0.5$ the DPD thermostat is not able to maintain constant temperature with the standard choice of weight functions. Taking, for example, weight functions as $\omega^R=\omega^D=\Theta(r_c-r)$ (see fourth column of Table I), the DPD thermostat maintains the temperature for a wall velocity interval $v_x \in [0,1]$, but also the normal pressure oscillations are suppressed.

B. Two opposing brushes

A system of two opposing brush layers was studied under constant shear. It is similar to that already studied in previous
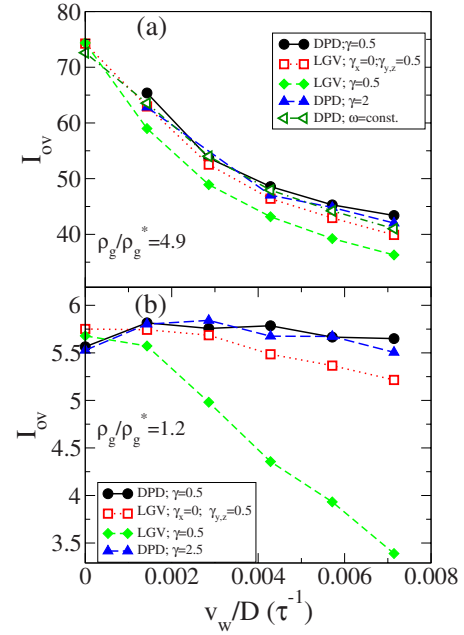

FIG. 7. (Color online) Overlap integral versus shear rate for the two studied grafting densities. For DPD, we used the standard weight functions [Eq. (10)] and the constant ones ($\omega=$const).

works [21–23,34–36], and originally attracted much interest because of its extraordinary small lateral friction forces. The equilibrium density profiles are depicted in Fig. 1(b). We considered brush layers of chains with $N=30$ beads at two different grafting densities, $\rho_g=1.2\rho_g^*$ and $\rho_g=4.9\rho_g^*$, where $\rho^*=1/\pi R_g^2$ ($R_g=3.02$ being the radius of gyration of a single chain in solution) is the grafting density characterizing the gradual crossover from the mushroom to the brush regime. $\rho_g=1.2\rho_g^*$ is a system within the crossover regime between mushroom and brush, whereas the latter choice of ρ_g leads to a semidilute brush [23]. For both considered grafting densities the opposing brushes interdigitated because the distance between the opposing end-grafted beads is $D=17.5<2h_0$ (h_0 denoting the unperturbed height of a single brush).

Following previous works [15,21,22], we quantify the amount of interdigitation via the overlap integral, I_{ov}, defined as

$$I_{\mathrm{ov}} \equiv v_{\mathrm{mono}} A \int_0^D \rho_l(z)\rho_u(z)dz, \qquad (13)$$

where ρ_u and ρ_l are, respectively, the number densities of upper and lower brush layers, $v_{\mathrm{mono}}=0.52$ is the volume of a monomer, and A is the surface area covered by the grafted beads. I_{ov} follows from integrating the curves depicted in the insets of Fig. 1. Figure 7 shows this quantity as a function of the shear rate, v_w/D, for good solvent conditions. The interdigitation is much higher for the larger grafting density, $\rho_g=4.9\rho_g^*$ [Fig. 7(a)], as expected from the more important stretching of the chains, and it becomes smaller with increasing shear rate and the progressive tilting of the chains. For the Langevin thermostat with $\gamma=0.5$ in all directions, this effect is more pronounced because the biasing of the flow profile increases the tilting of the brushes. A slight systematic
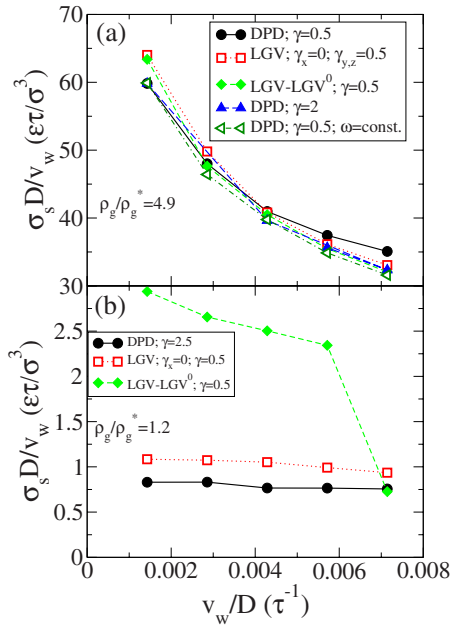
FIG. 8. (Color online) Comparison of "effective viscosity" for two opposing polymer brush layers under good solvent conditions for DPD and Langevin thermostats, using Langevin damping with $\gamma_x \neq 0$ and $\gamma_x = 0$. Different friction constants and two weight functions for DPD are considered. High and low grafting densities are presented in the upper and lower panels, respectively.

difference can also be observed for the DPD thermostat with $\gamma = 0.5$, where the overlap is systematically higher than in the other DPD cases. For $\gamma = 0.5$, the temperature is not properly conserved with the standard weight functions under good solvent conditions and the brush is additionally stretched.

On the other hand, for $\rho_g = 1.2 \rho_g^*$, the overlap is fairly constant for DPD and the Langevin thermostat with $\gamma_x = 0$ [Fig. 7(b)] over the whole interval of shear rates while for the standard Langevin thermostat ($\gamma_x \neq 0$) the strong monotonous decrease is again related to the bias in shear direction.

Figure 8(a) shows the shear stress $\sigma_s = \frac{\langle F_x \rangle}{A}$ ($\langle F_x \rangle$ the mean force acting on the end-grafted beads in shear direction) times the inverse shear rate as a function of the constant relative wall velocity, v_w, for good solvent conditions. As $\sigma_s D/v_w$ reflects the "effective viscosity" of the polymeric system, the decrease of this quantity indicates a nonlinear behavior, known as shear thinning. The overall behavior of all cases is roughly the same. The Langevin thermostat approximately reproduces the DPD result after subtracting the constant shear stress given by the Langevin damping [Eq. (12)] from the measured value. The Langevin thermostat with $\gamma_x = 0$ quantitatively agrees with the DPD case. The DPD thermostat was used with the standard weight functions for two different values of the friction constant, $\gamma = 2$ and $\gamma = 0.5$. The latter value was also used in combination with constant weight functions. Only for $\gamma = 0.5$, the standard weight functions lead to some systematic differences for the shear stress at large wall velocities. We found out that this is due to the fact that under these conditions DPD fails to maintain the temperature at the desired value ($T = 1.68$).

Figure 8(b) shows the effective viscosity for the smaller grafting density. The physical situation is now different as
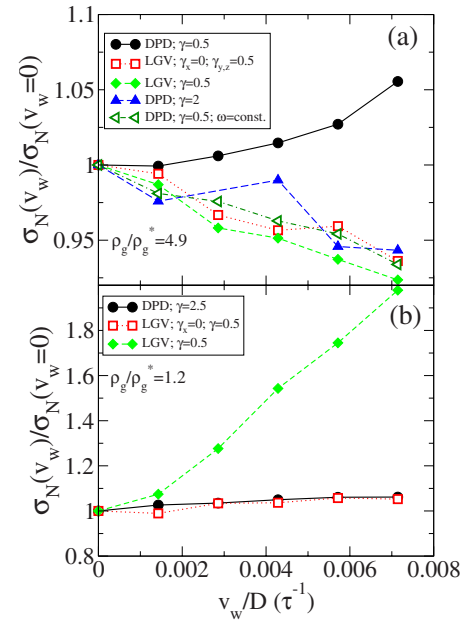

FIG. 9. (Color online) Comparison of normal pressure for two opposing polymer brush layers under good solvent conditions. DPD with different values of friction constants, γ, and weight functions are considered and compared to the standard Langevin thermostat (γ equal in all spatial directions) and the case $\gamma_x = 0$. The upper panel shows a grafting density with strong interdigitation between the brushes, and the lower one presents a case with small brush-brush interdigitation.

compared to the previous case: the opposing brush layers have a very small degree of interdigitation which is now independent of the wall velocity [see also Fig. 7(b)].

The linear response is observed for DPD and Langevin thermostats with $\gamma_x = 0$. For the standard Langevin thermostat ($\gamma_x \neq 0$), however, the "effective viscosity" decreases and drops drastically for the largest wall velocity. This can be explained via the behavior presented in Sec. III A: the tilting of the brush reduces the interdigitation of the brush layers not only because of the interaction among the brushes but also due to the strong interaction with the fictitious solvent that the Langevin thermostat inevitably implies. This is, however, an unphysical artifact in the simulations studied here. As a consequence, the density profiles depend on the parameters of the thermostat, which again is an unphysical effect. Moreover, we emphasize that, even when the overall behavior of DPD and Langevin thermostats with $\gamma_x = 0$ is similar, the absolute value of the shear stress is different.

Figure 9 shows the normal stress as a function of shear rate for the two studied grafting densities. Figure 9(a) considers the higher grafting density, for which the brushes are strongly interdigitated and slightly compressed (under good solvent conditions the mean force between the layers is repulsive). A decreasing normal stress as a function of shear velocity is found, except for the case of DPD with $\gamma = 0.5$ and the standard weight functions. As mentioned above, for this case DPD does not properly conserve temperature and a slight heat up of the system is observed, which in turn produces a further increase in the steady state stretching of the brush with a concomitant increase in the normal repulsion of
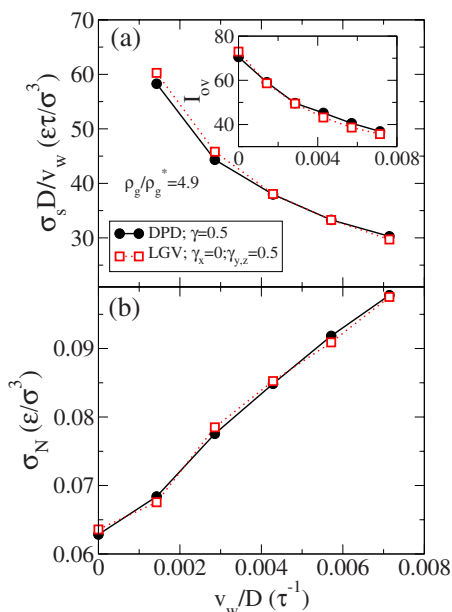
FIG. 10. (Color online) Comparison of shear and normal stress for DPD and Langevin thermostats with $\gamma_x=0$ (poor solvent conditions). Both thermostats give a similar result. The inset shows the overlap integral I_{ov} as defined in Eq. (13).
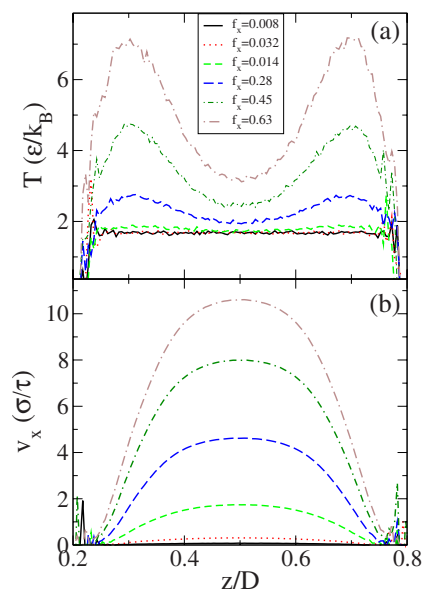

FIG. 11. (Color online) Poiseuille flow for different external forces, f_x. Upper panel: Temperature, as obtained from the mean square velocity perpendicular to the shear direction. Lower panel: Velocity profile across the polymeric liquid. Only the two smallest external forces, DPD with the standard weight functions [Eq. (10)], maintain the temperature at the desired value. The simulations were performed under poor solvent conditions.

the brush layers. For all the other cases, the decrease of normal pressure upon increasing velocity is produced by the progressive tilting of the chains and the decrease of interdigitation, already observed in the behavior of the overlap integral [Fig. 7(a)].

Figure 9(b) shows the normal stress for the smaller grafting density. Here, the brush is so dilute that the interaction between the brush layers is almost negligible. In this case, there is a mean attraction between the layers, due to the wall interaction with each bead [see Eq. (4)]. For DPD ($\gamma=2.5$) and the Langevin thermostat with $\gamma_x=0$, the structure of the brush is quite similar resulting in a similar behavior of the normal force. The small interdigitation leads to a very small change of the inclination angle giving rise to a very weak dependence of the normal stress on the wall velocity. This behavior agrees with the approximately constant behavior of the overlap integral shown in Fig. 7(b) and the linear response observed in the effective viscosity. A different behavior is found for the Langevin case with $\gamma=0.5$ in all directions. Under these conditions, the unphysical enhancement of the chain inclination leads to a much larger interaction between wall and monomers, which is mainly attractive for typical bead positions.

Normal and shear stresses were also investigated under poor solvent conditions. We used the Langevin thermostat with $\gamma=0.5$ perpendicular to the shear direction and $\gamma_x=0$. For the DPD thermostat with $\gamma=0.5$, the temperature is conserved under poor solvent conditions unlike in the good solvent case. As already shown in Table I, the larger cutoff radius for poor solvent conditions improves the DPD efficiency and keeps T constant even for the standard weight functions.

Figure 10(a) shows a very similar behavior of both thermostats concerning the effective viscosity, I_{ov}, and the nor-

mal stress. Within the considered regime of shear rates, both thermostat implementations lead to equivalent results. As compared with the good solvent case, the normal stress at the wall is negative, i.e., there is a mean attraction between upper and lower brush layers. This is due to the mean attraction among beads for this model.

If this equivalence between DPD and LGV with $\gamma_x=0$ holds also for stronger out-of-equilibrium situations, i.e., at higher shear velocities, remains to be investigated thoroughly.

C. The role of weight functions in the DPD thermostat

In this section we consider, in more detail, the ability of the DPD thermostat to conserve temperature in nonequilibrium simulations for different weight functions. The system under study is a polymeric liquid, formed by 10-bead chains, confined by two polymer brushes of identical chains [15]. The brush and melt density profiles across the perpendicular directions correspond to that of Fig. 1(c). We imposed either a Poiseuille flow by means of a constant external volume force or a linear Couette flow by moving the walls at constant relative velocity.

In Fig. 11, the violation of temperature conservation is shown as a function of external force, f_x, for Poiseuille flow using the standard DPD weight functions. The temperature, liquid number density, and brush grafting density were, respectively, set to $T=1.68$, $\rho_m=0.61$, and $\rho_g=5.5\rho_g^*(=0.77\sigma^{-2})$, with $\rho^*=1/\pi R_g^2$ and $R_g=1.50$. The typical Poiseuille velocity profile across the gap is shown in Fig. 11(b), while the temperature profile—measured by the mean
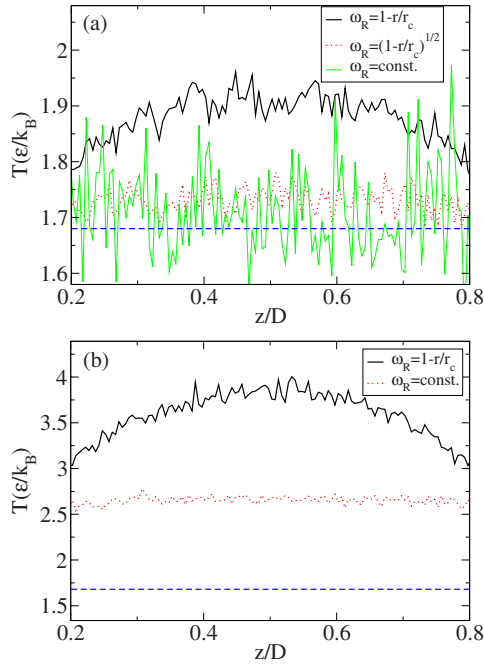
FIG. 12. (Color online) Comparison of different DPD weight functions for a Couette flow (poor solvent conditions). In the upper panel, $v_w=3$ is considered: while the standard choice of DPD weight functions is not able to conserve temperature, a choice of $\omega_R=\left(1-\frac{r}{r_c}\right)^{1/2}$ improves temperature conservation, and $\omega_R=\Theta(r_c-r)$ conserves temperature at the chosen value (indicated by the dashed line). At $v_w=8$ (lower panel), temperature is not conserved at the desired value, and the behavior across the film is very different for the considered weight functions (see the text).

square velocity in the direction perpendicular to the flow—is presented in Fig. 11(a). Temperature is conserved only for the two smallest forces. In the remaining cases, the temperature increases in the region of large velocity gradients. These cases show examples in which the DPD thermostat fails to maintain the desired temperature even under poor solvent conditions.

We also studied the temperature conservation for Couette flows using the weight functions considered in Table I. In Fig. 12(a) the temperature profiles for a shear velocity of $v_w=3$ are shown.

The standard weight functions clearly fail to keep temperature constant and lead to quadratic temperature profiles with a maximum in the middle of the gap. In contrast to the Poiseuille flow this is not related to the velocity gradient, which is constant across the gap for Couette flows. We attribute the resulting temperature profiles to the density distribution of monomers, which is enhanced close to the brush coated walls giving rise to a local improvement of the efficiency of the thermostat in this region. Another choice of weight functions $[\omega^R=\sqrt{\omega^D}=(1-r/r_c)^{1/2}]$ gives a better result although it also fails to conserve temperature. The constant-weight functions ($\omega^R=\sqrt{\omega^D}=1$) are more efficient and conserve temperature.

Figure 12(b) shows the temperature profile for a shear velocity of $v_w=8$. Under this condition, the thermostat is not able to conserve temperature because for reasonable values

of the friction constant energy cannot be dissipated as fast as it is plugged into the system. The solid line, corresponding to the standard DPD weight functions, shows a similar behavior as in the previous case: temperature is conserved more efficiently in the regions of higher density. For constant weight functions, temperature is fairly constant all across the film but differs from the desired value (indicated by a dashed line).

From these examples of strong out-of-equilibrium simulations, we conclude that the choice of weight functions can make an important difference. For example, the standard weight functions might not be able to conserve temperature even for a physically meaningful case. Constant weight functions seem to be a good alternative and are even more efficient computationally, as already noted in a previous study [7]. As a general guideline, it should be checked that the physical conditions fulfill the relation $\dot{\gamma}\ll N_{TP}\gamma_{DPD}/m$, where $\dot{\gamma}$ is the shear stress imposed to the system. In any case, for short-range potentials (as Lennard-Jones and good solvent conditions) or strong out-of-equilibrium simulations, the temperature profile across the sample, as shown in Fig. 12, can give insight on the ability of the thermostat for keeping the temperature constant.

IV. CONCLUSIONS

In this work we tested and compared commonly used implementations of Langevin and DPD thermostats for different polymeric systems. Equilibrium, transient and steady state conditions were considered for the study of various reference systems, such as polymer brush bearing surfaces or brush-melt interfaces. We utilized a well-studied coarse-grained bead-spring polymer model. By varying the cutoff in the interaction potential we mimicked good and poor solvent conditions. We quantified the relative strength of the thermostats in a wide range of friction constants, γ, and found that the strength of the Langevin thermostat is much larger than DPD with standard weight functions for similar values of γ. The simulation of the transient state of a polymer brush layer driven to constant velocity from rest illustrates the known weaknesses of the Langevin thermostat—lack of momentum conservation, screening of hydrodynamic interactions, and violation of Galilean invariance—and how these are avoided by the DPD thermostat which conserves local momentum. When applied in shear direction, the Langevin thermostat biases the velocity profile. The common work-around of switching off the Langevin thermostat in the nonequilibrium direction was analyzed for different systems. We found that, in most cases, the latter behaves similar to the DPD scheme but care must be exerted when the system is strongly driven out of equilibrium.

We furthermore quantified the differences between various forms of weight functions of the DPD thermostat, which can be chosen freely, provided that the weights for random and dissipative forces obey relation (8). It is important to note that most of the previous works using DPD utilized a standard form [Eq. (10)] which was originally intended to be used in conjunction with "soft" potentials. When the DPD thermostat is applied to typical coarse-grained potentials, the

"hard" nature of the conservative potentials prevents one from using a very large time step, and therefore not much is gained from "smooth" thermostat forces. Moreover, we found that the typical weights can be regarded as adequate for equilibrium and slightly out-of-equilibrium conditions but they fail to conserve temperature for medium and strong driving forces. We tested this for both, Poiseuille and Couette flows, of a polymer melt confined between two polymer brush layers. We found quantitatively that taking constant weight functions is both computationally faster and yields a thermostat that is more suitable for strong out-of-equilibrium situations in which a large amount of heat per unit time is produced.

It is important to note that none of the methods discussed in the present paper are suitable to fully account for hydrodynamic effects at arbitrary densities. For instance, the coupling between the monomer density distribution and the external flow profile is not described. To achieve this, other methods, e.g., the self-consistent solution of the Brinkman equation [37] must be applied. In a future study we plan to investigate the systems considered here using explicit solvent molecules. This should put us in a position to understand the importance of the effects delineated above.

Finally, our results clearly show that great care is needed in nonequilibrium MD simulations of soft matter systems in order to ensure that the simulations are free of artifacts due to an inappropriate choice of the thermostat.

[1] M. P. Allen and D. J. Tildesley, *Computer Simulation of Liquids* (Clarendon, Oxford, 1990).

[2] The regime in which the accelerations are kept and are integrated explicitly is in general called stochastic dynamics. Alternatively, if friction and random forces are big enough, the instantaneous values of the accelerations can be set to zero. This is typically referred to as Brownian dynamics.

[3] P. H. Hünenberger, Adv. Polym. Sci. **173**, 105 (2005).

[4] G. Grest, Adv. Polym. Sci. **138**, 1 (1999).

[5] N. V. Priezjev, A. A. Darhuber, and S. M. Troian, Phys. Rev. E **71**, 041608 (2005).

[6] N. V. Priezjev and S. M. Troian, Phys. Rev. Lett. **92**, 018302 (2004).

[7] T. Soddemann, B. Dünweg, and K. Kremer, Phys. Rev. E **68**, 046702 (2003).

[8] B. Smit and D. Frenkel, *Understanding Molecular Simulation*, 2nd ed. (Academic, New York, 2002).

[9] P. J. Hoogerbrugge and J. M. V. A. Koelman, Europhys. Lett. **19**, 155 (1992).

[10] P. Español and P. Warren, Europhys. Lett. **30**, 191 (1995).

[11] P. Español, Phys. Rev. E **52**, 1734 (1995).

[12] R. D. Groot and P. B. Warren, J. Chem. Phys. **107**, 4423 (1997).

[13] B. Dünweg, J. Chem. Phys. **99**, 6977 (1993).

[14] T. A. Thompson and M. O. Robbins, Phys. Rev. A **41**, 6830 (1990).

[15] C. Pastorino, K. Binder, T. Kreer, and M. Müller, J. Chem. Phys. **124**, 064902 (2006).

[16] I. Vattulainen, M. Karttunen, G. Besold, and J. M. Polson, J. Chem. Phys. **116**, 3967 (2002).

[17] G. Besold, I. Vattulainen, M. Karttunen, and J. M. Polson, Phys. Rev. E **62**, R7611 (2000).

[18] I. Pagonabarraga, M. H. Hagen, and D. Frenkel, Europhys. Lett. **42**, 377 (1998).

[19] G. S. Grest and K. Kremer, Phys. Rev. A **33**, 3628 (1986).

[20] M. Müller and L. G. MacDowell, Europhys. Lett. **55**, 221 (2001).

[21] T. Kreer, M. H. Müser, K. Binder, and J. Klein, Langmuir **17**, 7804 (2001).

[22] T. Kreer, K. Binder, and M. H. Müser, Langmuir **19**, 7551 (2003).

[23] T. Kreer, S. Metzger, M. Müller, K. Binder, and J. Baschnagel, J. Chem. Phys. **120**, 4012 (2004).

[24] L. G. MacDowell and M. Müller, J. Chem. Phys. **124**, 084907 (2006).

[25] J. Klein, D. Perahia, and S. Warburg, Nature **352**, 143 (1991).

[26] J. Klein, E. Kumacheva, D. Mahalu, D. Perahia, and L. J. Fetters, Nature **370**, 634 (1994).

[27] M. Kröger, Phys. Rep. **390**, 453 (2004).

[28] J. Baschnagel and F. Varnik, J. Phys.: Condens. Matter **17**, R851 (2005).

[29] B. Dünweg and K. Kremer, J. Chem. Phys. **99**, 6983 (1993).

[30] L. González MacDowell, M. Müller, C. Vega, and K. Binder, J. Chem. Phys. **113**, 419 (2000).

[31] M. Müller and L. G. MacDowell, Macromolecules **33**, 3902 (2000).

[32] M. Müller and L. González MacDowell, J. Phys.: Condens. Matter **15**, R609 (2003).

[33] S. Barsky and M. O. Robbins, Phys. Rev. E **63**, 021801 (2001).

[34] P. Y. Lai and K. Binder, J. Chem. Phys. **97**, 586 (1992).

[35] P. Y. Lai and K. Binder, J. Chem. Phys. **98**, 2366 (1993).

[36] K. Binder, P. Y. Lai, and J. Wittmer, Faraday Discuss. **98**, 97 (1994).

[37] H. C. Brinkman, Appl. Sci. Res., Sect. A **1**, 27 (1949).